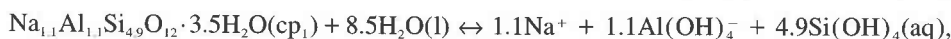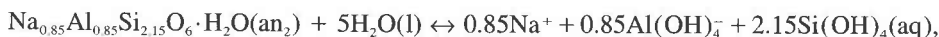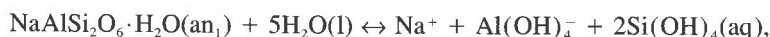# Solubility and stability of zeolites in aqueous solution: I. Analcime, Na-, and K-clinoptilolite

R.T. WILKIN* AND H.L. BARNES

Ore Deposits Research Section, Pennsylvania State University, University Park, Pennsylvania 16802, U.S.A.

ABSTRACT

The solubilities of analcime and clinoptilolite were determined in dilute, weakly alkaline, aqueous solutions below 300 °C and at vapor-saturated pressures. Analcimes used in this study were from Mont St. Hilaire, Quebec (an_1, Si/Al = 2.02) and Wikieup, Arizona (an_2, Si/Al = 2.55); clinoptilolite samples were from Castle Creek, Idaho (Si/Al = 4.50). The effects of alkali content (Na,K) on clinoptilolite solubility were determined by using cation-exchanged varieties of the Castle Creek material (cp_1, cp_2). In neutral to weakly alkaline solutions, the dominant solubility-controlling reactions of these zeolites are

$$NaAlSi_2O_6 \cdot H_2O(an_1) + 5H_2O(l) \leftrightarrow Na^+ + Al(OH)_4^- + 2Si(OH)_4(aq),$$

$$Na_{0.85}Al_{0.85}Si_{2.15}O_6 \cdot H_2O(an_2) + 5H_2O(l) \leftrightarrow 0.85Na^+ + 0.85Al(OH)_4^- + 2.15Si(OH)_4(aq),$$

$$Na_{1.1}Al_{1.1}Si_{4.9}O_{12} \cdot 3.5H_2O(cp_1) + 8.5H_2O(l) \leftrightarrow 1.1Na^+ + 1.1Al(OH)_4^- + 4.9Si(OH)_4(aq),$$

and

$$K_{1.1}Al_{1.1}Si_{4.9}O_{12} \cdot 2.7H_2O(cp_2) + 9.3H_2O(l) \leftrightarrow 1.1K^+ + 1.1Al(OH)_4^- + 4.9Si(OH)_4(aq).$$

The logarithm of the equilibrium constants of these reactions were fit to the function: log $K = A + BT + C/T + D \log T$. At 25 °C, log K_{25} values for the Mont St. Hilaire analcime, Wikieup analcime, Na-clinoptilolite, and K-clinoptilolite are −16.1, −15.0, −26.5, and −28.1, respectively. These data were combined with the thermodynamic properties of the aqueous (aq) species $Si(OH)_4$, $Al(OH)_4^-$, Na^+, K^+, and liquid water (l) to determine standard Gibbs free energies of formation as a function of temperature. Values of ΔG_f^0 at 25 °C and 1 bar for the Mont St. Hilaire analcime and Wikieup analcime are −3089.2 and −3044.4 kJ/mol, respectively. The ΔG_f^0 values for hydrous Na-clinoptilolite and K-clinoptilolite, respectively, are −6267.9 and −6107.4 kJ/mol at 25 °C and 1 bar. The solubility data reported here, and results obtained from previous calorimetric studies, indicate that the aluminosilicate frameworks of analcime and clinoptilolite are stabilized by an increase in Al content.

INTRODUCTION

Zeolites are widespread authigenic aluminosilicates that form during water-rock interactions below roughly 300 °C and 2 kbars. The predominant geologic settings where zeolites form (Hay 1978) are (1) deep-sea pelagic sediments (e.g., Kastner and Stonecipher 1978; Gingele and Schulz 1993), (2) near-surface environments where alkaline meteoric waters interact with volcanic rocks (e.g., Sheppard and Gude 1969; Surdam and Sheppard 1978), (3) geothermal regions (e.g., Kristmannsdottir and Tomasson 1978), and (4) under low-grade metamorphic conditions (e.g., Iijima and Utada 1966).

Analcime and clinoptilolite are common in all of these zeolite-forming environments and are among the most abundant zeolites in nature (e.g., Gottardi and Galli

1985). The prevalence of analcime and clinoptilolite in the rhyolitic tuffs at Yucca Mountain, Nevada, a potential repository for high-level radioactive wastes, has recently stimulated research on their physico-chemical properties (e.g., Bish 1984; Bowers and Burns 1990; Pabalan 1994; Gunter et al. 1994; Murphy et al. 1996; Carey and Bish 1996). Clinoptilolite at Yucca Mountain is particularly important because of its hydration/dehydration behavior, its potential to breakdown to analcime, and its cation-exchange properties and potential for immobilizing radio-nuclide cations, such as Cs and Np. The precipitation of these zeolites directly affects the permeability of volcanics and sediments because of their normal distribution as fracture fillings so that an understanding of their stability is an important factor in evaluating the permeabilities of their host rocks. However, predicting the extent of diagenetic and low-grade metamorphic reactions of zeolites and other clay minerals has been impeded by insufficient

thermodynamic data to account for their large variations in Si/Al, H_2O, and cation contents. Because zeolite assemblages in tuffaceous sediments and other geologic environments apparently represent non-equilibrium assemblages, as we shall show later in this paper, kinetic factors that control rates of dissolution and precipitation are of paramount importance in understanding the formation and evolution of zeolite-bearing mineral assemblages during continued water-rock interaction.

Various analytical techniques have been used to garner many physico-chemical properties of zeolites. For example, NMR spectroscopy to determine Si-Al ordering (e.g., Phillips and Kirkpatrick 1994; Ward and McKague 1994); neutron diffraction and X-ray powder diffraction to determine cell parameters (e.g., Stahl et al. 1990; Armbruster and Gunter 1991; Bish 1984, 1988); thermogravimetric analyses and differential scanning calorimetry to evaluate dehydration/hydration behavior (e.g., Simonot-Grange 1979; Carey and Bish 1996); and mass spectroscopy to study zeolite-H_2O exchange mechanisms (e.g., Feng and Savin 1993; Noto and Kusakabe 1997). Thermodynamic data obtained from calorimetric measurements on the zeolites analcime, clinoptilolite, heulandite, mesolite, mordenite, natrolite, phillipsite, scolecite, stilbite, leonhardite, laumontite, yugawaralite, and faujasite are reported in Johnson et al. (1982, 1983, 1985, 1991, 1992), Hemingway and Robie (1984), Howell et al. (1990), Kiseleva et al. (1996a, 1996b), and Petrovic and Navrotsky (1997). Measuring zeolite solubilities in aqueous solutions has been avoided in the past because of uncertainties in aqueous speciation, expected formation of secondary phases, and slow reaction rates below 200 °C (e.g., Johnson et al. 1982). However, solubility measurements on zeolite powders free of excess strain and ultra-fine particles are a comparatively direct method to evaluate thermodynamic properties of zeolite minerals while ensuring a buffered hydration state. Here we report the aqueous solubilities of a high-Si sedimentary analcime (Wikieup, Arizona) from 25–225 °C, a low-Si hydrothermal analcime (Mont St. Hilaire, Quebec) from 25–300 °C, and Na- and K-exchanged clinoptilolite (Castle Creek, Idaho) from 25–265 °C, all at vapor-saturated pressures. The results of these solubility experiments provide a new set of standard Gibbs free energies of formation for these minerals as a function of T, as well as a basis for relating measurements of dissolution and precipitation rates to departures from equilibrium (Wilkin and Barnes 1997).

SOLUBILITY STUDIES

Materials selection and pretreatment

Analcime grains from Mont St. Hilaire, Quebec, Canada, a hydrothermal deposit, and Wikieup, Arizona, U.S.A, a sedimentary deposit, were used in our solubility experiments. These analcimes formed under contrasting physicochemical conditions and are an approximately stoichiometric (Si/Al $\sim$ 2) and highly siliceous (Si/Al $\sim$ 2.5)
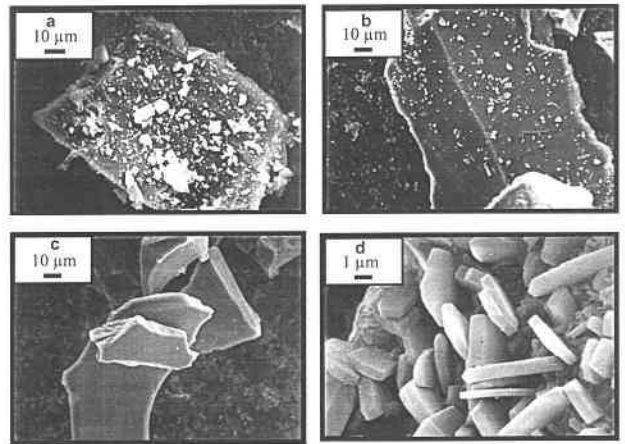

FIGURE 1. SEM photomicrographs of (**a**) Mont St. Hilaire analcime after crushing and seiving; (**b**) Mont St. Hilaire analcime after ultra-sonic cleaning; (**c**) Mont St. Hilaire analcime after hydrothermal treatment (120 °C for 2 weeks); note analcime grains are free of ultra-fine particles; and (**d**) hydrothermally treated Na-clinoptilolite.

analcime, respectively. The clinoptilolite from Castle Creek, Idaho, U.S.A., was generously donated by F. Aplin of Pennsylvania State University. Because of their high zeolite content (>95%), bulk materials from the Castle Creek deposit required a minimum of physical separations.

The Mont St. Hilaire analcime was purchased from Ward's Scientific. Approximately 200 grams of analcime grains were hand-picked to be free of visible dark crystals of acmite, carefully crushed in an agate mortar, and sieved to recover the 75–125 μm size fraction. The analcime powder was then repeatedly washed with doubly distilled and deionized water in an ultrasonic cleaner to remove adhered ultra-fine particles. In addition, we found it necessary to recrystallize the zeolites hydrothermally by aging them at $\sim$125 °C with a high solid/water ratio and near-neutral pH for several weeks. This method resulted in mineral powders free of ultra-fine particles having high surface energies, which increase both mineral solubility and dissolution rates. Furthermore, the recrystallized product has a surface devoid of the etch pits, surface strain, and leached surfaces typically produced by harsh chemical pretreatment and particle sizing. The high solid/water ratio minimized any leaching of the surfaces of the mineral grains.

The final cleaned and recrystallized powder was examined by X-ray diffraction (XRD; Rigaku Geigerflex) to determine mineral content, and by scanning electron microscopy (SEM; ISI SX-40A) to determine particle morphology and uniformity of particle size. The pretreatment procedures described above result in materials that are ideal for both solubility and kinetic experimental studies (Fig. 1).

Major element abundances were determined by inductively coupled plasma emission spectroscopy (ICPES; Leeman Labs PS3000) after lithium metaborate fusion

TABLE 1. Chemical analyses and structural formulae for the analcime and clinoptilolite samples used in this study

	Mont St. Hilaire analcime	Wikieup analcime	Castle Creek clinop- tilolite	Castle Creek Na- clinop- tilolite	Castle Creek K-clinop- tilolite
SiO$_2$	55.15	58.68	65.50	64.75	64.65
TiO$_2$	<0.02	0.07	0.08	0.08	0.09
Al$_2$O$_3$	23.16	19.49	12.40	12.20	12.20
Fe$_2$O$_3$	<0.02	0.77	0.48	0.90	0.55
MgO	<0.02	0.23	1.07	0.07	0.05
CaO	0.10	0.17	0.72	0.06	0.05
MnO	0.01	0.01	<0.01	0.01	0.01
Na$_2$O	14.03	12.09	3.57	7.26	0.08
K$_2$O	0.10	0.30	2.34	0.24	10.87
H$_2$O	8.12	8.54	12.90	13.85	10.43
Total	100.63	100.35	99.06	99.51	98.98
n	(4)	(2)	(1)	(2)	(2)
Si	2.01	2.14	4.91	4.90	4.91
Al	0.99	0.84	1.08	1.09	1.09
Mg	0.00	0.01	0.12	0.00	0.00
Ca	0.00	0.01	0.06	0.00	0.00
Na	0.99	0.86	0.52	1.07	0.01
K	0.00	0.01	0.21	0.02	1.05
H$_2$O	0.99	1.04	3.28	3.48	2.65
Si/Al	2.02	2.55	4.55	4.50	4.50

Note: n = number of analyses. Number of cations normalized to 6 and 12 O atoms for analcime and clinoptilolite, respectively.

and dissolution in 5% HNO$_3$. Analytical accuracy and precision of the ICPES measurements are within 3% at the 2σ confidence level, based on analytical reproducibility of NIST-traceable standards and conventional rock and mineral standards. The H$_2$O content of the zeolites at room temperature and 50% relative humidity was determined by heating at 900 °C for 2 h and measuring the weight loss of samples that were previously equilibrated over a saturated Ca(NO$_3$)$_2$ solution. Duplicate and triplicate measurements agreed to ±3%. The H$_2$O content of the Mont St. Hilaire analcime was also determined by thermogravimetric analyses (TGA) in static air using a TA Instruments 2050 unit. TGA scans were run on ~25 mg samples from 25 to 800 °C at a heating rate of 10 °C per minute. Analytical data and the calculated composition of the Mont St. Hilaire analcime are shown in Table 1 and indicate a nearly stoichiometric composition with Si/Al = 2.02.

About 10 g of analcime from Wikieup was donated by D. Bish (Los Alamos National Laboratory). This analcime was used as received, and we characterized it with the above techniques (Table 1). The composition of this sedimentary analcime is distinctly non-stoichiometric with a Si/Al ratio of 2.55, similar to analcime found in the volcanic tuffs at Yucca Mountain (Broxton et al. 1987).

Material from the Castle Creek deposit consists almost entirely of clinoptilolite (Mondale et al. 1988) with only about 5% of impurities, mainly smectitic clay with some opal CT. The bulk material was crushed in an agate mortar and sieved through a 100 μm screen. To remove the

smectite, about 50 g of the sieved material was placed in a 1 L graduated cylinder along with a magnetic stirring bar and distilled, deionized H$_2$O. The contents of the cylinder were stirred for about 10 min, then the suspension was allowed to settle for nearly 5 min before decanting the overlying fluid. The process was repeated several times. The supernatant fluid was enriched in a mixed-layer clay (~90% smectite, 10% illite) and very fine-grained clinoptilolite (<3 μm).

We used the cation exchange properties of clinoptilolite to prepare Na-clinoptilolite to simplify the interpretation of the solubility results and to obtain thermodynamic data on phases having near end-member compositions. About 150 g of purified clinoptilolite was treated with 500 mL of 5 m NaCl (Baker reagent grade) at 120 °C for approximately 1000 h. The NaCl solution was refreshed six times during the Na-exchange treatment. The final material was washed repeatedly with distilled, deionized H$_2$O and dried under high humidity at 60 °C, and then allowed to equilibrate with ambient humidity at room temperature. A similar cation exchange experiment was performed to prepare K-clinoptilolite. Again, about 150 g of the purified clinoptilolite was treated with 500 mL of 3 m KCl.

The major element compositions and structural formulae of the Na- and K-clinoptilolite and original, unexchanged clinoptilolite are given in Table 1. Ca^{2+} and Mg^{2+} were largely removed during the exchange, and near end-member Na- and K-clinoptilolite were produced. Note that the H$_2$O contents in monovalent Na- and K-clinoptilolites (Table 1) are different because of differences in the hydration energies of the exchangeable cations (e.g., Boles 1972; Bish 1988).

Laboratory procedures

The hydrothermal solubilities of Mont St. Hilaire analcime and Na- and K-clinoptilolite were measured using Ti-17 alloy or gold-plated, stainless steel autoclaves (nominal volume 1100 mL) contained in a rocking, dual-wound furnace (Barnes 1971; Bourcier and Barnes 1987). Pressure was measured using a Heise Bourdon tube pressure gauge accurate to within ±0.1% of full scale. Temperature was monitored and controlled using two premium quality, chromel-alumel thermocouples (Thermo-electric Company) inserted into the top and bottom of the autoclave. The thermocouples were calibrated by measurement of vapor P over pure H$_2$O and with a platinum-resistance thermometer read with a Mueller bridge, DC power supply, and galvanometer. The Mueller bridge measures resistance to ±0.0005Ω corresponding to a sensitivity of about ±0.005 °C. The 2σ uncertainty in the T reported here is ±1.5 °C. Experiments were conducted at P along the liquid-vapor curve of the aqueous solutions.

At the beginning of an experiment, 30–50 g of zeolite powder was placed in the autoclave along with about 400 mL of doubly distilled H$_2$O purged with nitrogen gas to remove CO$_2$ and O$_2$. The autoclave was then flushed with nitrogen gas, sealed, and placed in the furnace. Next,

TABLE 2. Logarithm of the ionization constants used in this study

Reaction	25°	50°	90°	125°	175°	200°	225°	265°	275°	300°	Ref.
$H_2O_{(l)} = H^+ + OH^-$	−13.99	−13.27	−12.44	−11.91	−11.48	−11.31	−11.26	−11.24	−11.27	−11.33	(1)
$Al^{3+} + OH^- = Al(OH)^{2+}$	9.0	8.8	8.8	9.1	9.9	10.4	11.0	11.9	12.2	12.9	(2, 1)
$Al^{3+} + 2OH^- = Al(OH)_2^+$	17.8	17.6	17.8	18.1	18.9	19.4	20.0	21.1	21.4	22.2	(2, 1)
$Al^{3+} + 3OH^- = Al(OH)_3$	25.8	25.9	26.2	26.6	27.6	28.0	28.7	29.7	30.1	30.8	(2, 1)
$Al^{3+} + 4OH^- = Al(OH)_4^-$	33.8	33.1	32.7	32.7	33.5	33.9	34.6	36.0	36.4	37.4	(2, 1)
$Na^+ + Al(OH)_4^- = NaAl(OH)_4$	−0.10	0.07	0.29	0.48	0.74	0.87	1.02	1.31	1.38	1.58	(3)
$H_4SiO_4 = H_3SiO_4^- + H^+$	−9.83	−9.49	−9.16	−8.98	−8.85	−8.87	−8.92	−9.03	−9.08	−9.20	(4)
$NaOH = Na^+ + OH^-$	0.75	0.74	0.68	0.56	0.25	0.08	−0.15	−0.82	−0.99	−1.42	(5)

Note: Data sources (1) Busey and Mesmer (1978); (2) Bourcier et al. (1993); (3) Diakonov et al. (1996); (4) Busey and Mesmer (1977); (5) Pokrovskii and Helgeson (1995).

rocking was begun to ensure mixing between the solution and solids and to minimize T gradients in the autoclave. The system was maintained generally for several days at a constant T where the solubility was to be determined. Solubility measurements were made by approaching equilibrium both from undersaturation and also from supersaturation by either increasing or decreasing T, and by taking multiple samples at a single T over increasing intervals of time. Experiments were typically conducted by first ramping up T, making a series of isothermal stops, and then ramping down T to examine the approach to equilibrium from supersaturation. Solution sampling was carried out at various T and P using a double-valve configuration (e.g., Gammons and Barnes 1989). Approximately 8 mL of solution were collected into a plastic syringe and filtered through a 0.2 μm cellulose acetate, syringe filter (Nalgene). Room temperature pH was measured on a 3 mL aliquot with a semi-micro combination electrode (Corning) calibrated with NIST-traceable standard buffers. The remaining filtered solution was diluted with doubly distilled, deionized H_2O and Ultrex HNO_3. Solutions were analyzed for total Si, Al, and Na or K by ICPES. With these methods, analytical precision and accuracy was better than ±5%. The measured concentrations of Si, Al, Na, and K in replicate samples also generally agreed to ±5%.

At the end of an experiment, the autoclave was opened and the contents washed with water and then dried. In most cases, powder XRD and SEM analyses did not reveal formation of secondary phases during the solubility experiments. However, we could not determine the solubility product of clinoptilolite at T above 265 °C because the high concentrations of aqueous silica generated by the dissolving clinoptilolite led to the precipitation of quartz along the vapor-liquid interface within the autoclave.

The solubility of Wikieup analcime was measured at 90, 125, 175, and 225 °C using sealed silica tubes placed within a rocking furnace. The methods used to study the analcime differ from those used to study clinoptilolite because of the relatively small amount of material available. Approximately 500 mg of the analcime plus ~10 mL of N_2-purged doubly distilled, deionized H_2O were placed in a silica tube sealed at one end. The tube was then flushed with argon gas, sealed, and placed in the furnace that was rocked to ensure mixing between solid and solution in

the silica tubes. After several days, a tube was taken from the furnace, quenched in ice water, and cracked open. Then the solution was filtered and measurements made of pH, Si, Al, and Na concentrations. In these experiments, because of its contribution to the total concentration of silica, the silica tube can be regarded as a buffer of aqueous silica concentrations.

Below 100 °C, some experiments were conducted in 30 mL polyethylene bottles. In these experiments, T was maintained at 50 ± 2 °C in a furnace or at room temperature, 22 ± 4 °C. The bottles were loaded with approximately 2 g of zeolite and about 20 mL of a 5 mm sodium borate (potassium borate) plus 7 mm HCl stock solution. The HCl was added to the solution to maintain a pH below the first ionization constant of silicic acid. The suspensions were mixed by frequently (daily) inverting the bottles several times. From these bottles, fluid samples were collected and filtered through 0.2 μm syringe filters, and then analyzed using the methods described above. In these low-temperature experiments, zeolite solubilities were approached from undersaturation only.
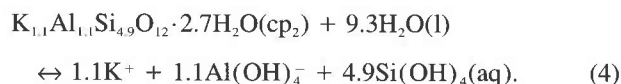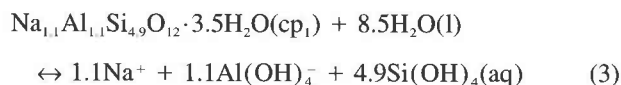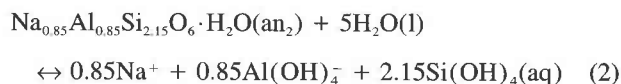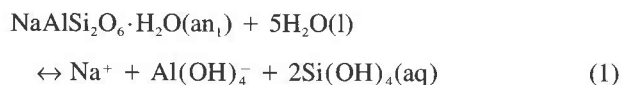
Evaluation of experimental data

Calculation of thermodynamic solubility products from the measured concentrations of ΣAl, ΣNa, and ΣSi in equilibrium with the zeolites requires knowing the dominant, stoichiometrically balanced, dissolution reaction, a method of partitioning total analytical concentrations into the appropriate aqueous speciation, and an ion activity model to calculate activity coefficients for all aqueous species. The solutions were speciated at T using the selected thermodynamic constants listed in Table 2. Individual ion activity coefficients were calculated using the "B-dot" method of the extended Debye-Hückle equation with parameters from Helgeson and Kirkham (1974). Because buffered solutions were not utilized in the high-temperature experiments to control pH, solution ionic strengths were derived solely from the products of dissolution and, consequently, remained low, resulting in small activity corrections. For the neutral species, $Si(OH)_4$, activity coefficients were taken to be unity. Only monomeric species of Al and Si were considered to be present in the solutions.

Several recent investigations have shown that in slightly alkaline solutions, soluble Al occurs dominantly as

$Al(OH)_4^-$ (e.g., Wesolowski 1992; Castet et al. 1993; Bourcier et al. 1993; Wesolowski and Palmer 1994). At high temperatures and in concentrated NaOH solutions, the sodium aluminate ion, $NaAl(OH)_4$, also requires consideration (Pokrovskii and Helgeson 1995; Diakonov et al. 1996), although in this study the complex apparently never constituted more than 5–10% of ΣAl.

At the measured pH of all solutions collected (6.8–9.3 at 25 °C), aqueous Al and Si species were dominantly $Al(OH)_4^-$ and $Si(OH)_4$, respectively. Thus, the solubility product, K, or the more general ion activity product, Q, for Mont St. Hilaire analcime (an_1), Wikieup analcime (an_2), Na-clinoptilolite (cp_1), and K-clinoptilolite (cp_2) can be determined most accurately from the following stoichiometric dissolution/precipitation reactions:

$$NaAlSi_2O_6 \cdot H_2O(an_1) + 5H_2O(l)$$

$$\leftrightarrow Na^+ + Al(OH)_4^- + 2Si(OH)_4(aq) \quad (1)$$

$$Na_{0.85}Al_{0.85}Si_{2.15}O_6 \cdot H_2O(an_2) + 5H_2O(l)$$

$$\leftrightarrow 0.85Na^+ + 0.85Al(OH)_4^- + 2.15Si(OH)_4(aq) \quad (2)$$

$$Na_{1.1}Al_{1.1}Si_{4.9}O_{12} \cdot 3.5H_2O(cp_1) + 8.5H_2O(l)$$

$$\leftrightarrow 1.1Na^+ + 1.1Al(OH)_4^- + 4.9Si(OH)_4(aq) \quad (3)$$

$$K_{1.1}Al_{1.1}Si_{4.9}O_{12} \cdot 2.7H_2O(cp_2) + 9.3H_2O(l)$$

$$\leftrightarrow 1.1K^+ + 1.1Al(OH)_4^- + 4.9Si(OH)_4(aq). \quad (4)$$

The standard state adopted in this study is unit activity for pure minerals and fluids at the T and P of interest. The standard state for aqueous species is unit activity at the T and P of interest for an ideal one molal solution. Following these standard state conventions, the ion activity product with respect to reaction 1, Q_1, can be computed using the equation:

$$\log Q_1 = \log a_{Na^+} + \log a_{Al(OH)_4^-} + 2 \log a_{Si(OH)_4} \quad (5)$$

where a_i denotes the activity of an aqueous species, i, and at equilibrium, $Q_1 = K_1$. Similar expressions can be derived for ion activity products with respect to reactions 2–4. Note that the apparent ion activity products or solubility products are independent of the hydration state of the zeolites where H_2O has unit activity. The hydration number affects directly the stoichiometric coefficient of molecular H_2O in reactions 1–4; consequently, as discussed further below, an accurate hydration number at T and P along the liquid-vapor curve of H_2O is required to extract standard thermodynamic constants of the zeolites.

To ensure charge balance in reactions 1–4, the stoichiometric cation proportion, either Na or K, of analcime and clinoptilolite has been set equal to the stoichiometric proportion of Al. For the Na-clinoptilolite, the contribution of K and other alkali elements have been taken as negligible and are neglected in the calculation of the solubility product. The molar [Na/(Na+K)], [Na/(Na+Ca)], and [Na/(Na+Mg)] values of the Na-clinoptilolite used in this study are 0.98, 0.99, and 0.99, respectively; thus,
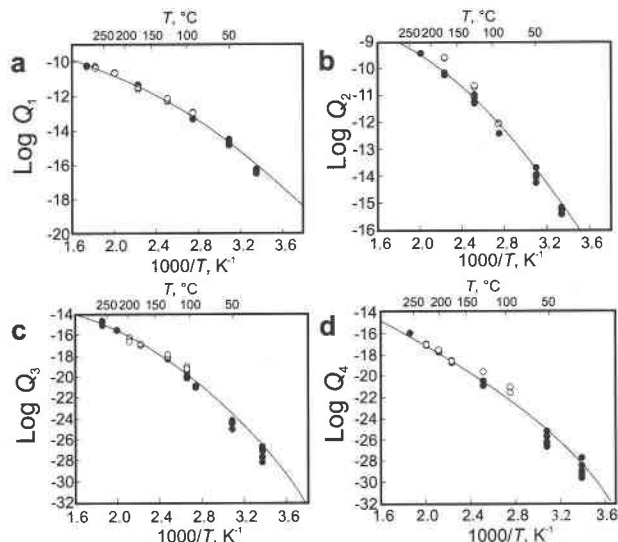

FIGURE 2. Log Q vs. $1000/T$ plots for (a) Mont St. Hilaire analcime; (b) Wikieup analcime; (c) Castle Creek Na-clinoptilolite; and (d) Castle Creek K-clinoptilolite. Filled circles indicate sampling from undersaturation; open circles indicate sampling from supersaturation.

errors accrued by omitting the contribution of these elements to the solubility product are negligible compared to other experimental and analytical uncertainties.

RESULTS AND DISCUSSION

The data from the zeolite solubility vs. T measurements are shown in Figure 2. Above 100 °C, zeolite solubilities were determined at P equivalent to the saturated vapor pressure of the solutions; below 100 °C, solubilities were determined at 1 bar. In Figure 2, the direction of approach to the conditions of each solubility measurement is shown from either undersaturation or supersaturation. Below 100 °C, solubilities were determined mostly from undersaturated conditions. Above 100 °C, however, solubilities were approached from both directions because of substantially increased rates of dissolution and precipitation at elevated T. The temperature-dependent log Q values and their standard errors were calculated by averaging the set of ion activity products determined at each T (Table 3). In Appendix Tables 1 and 2, experimental data are tabulated including: experiment temperature; experiment duration; concentrations of ΣSi, ΣAl, and ΣNa; pH; direction of sampling approach; and calculated log Q for each sampling interval. Steady-state solubility values are a direct measurement of the standard free energy change of the dissolution or precipitation reaction (ΔG_r^0) and were used to derive thermodynamic quantities as discussed below.

For the dissolution reactions of both analcime and clinoptilolite, the calculated values of log Q increase with increasing T indicating a positive enthalpy of reaction, ΔH_r^0. Because the log Q values do not depend linearly on $1/T$ (Fig. 2), the enthalpies of reaction must vary over the

TABLE 3. Average log Q values for reactions 1–4

T (°C)	Mont St. Hilaire analcime log Q_1	Wikieup analcime log Q_2	Castle Creek Na-clinoptilolite log Q_3	Castle Creek K-clinoptilolite log Q_4
25	−16.21 (±0.27)	−15.36 (±0.24)	−26.96 (±0.54)	−28.85 (±0.64)
50	−14.75 (±0.17)	−13.99 (±0.19)	−24.48 (±0.19)	−26.18 (±0.51)
90	−13.02 (±0.26)	−12.24 (±0.21)	−21.17 (±0.06)	−21.37 (±0.24)
100	—	—	−19.55 (±0.43)	—
125	−12.14 (±0.16)	−11.15 (±0.25)	−18.54 (±0.45)	−20.33 (±0.50)
175	−11.50 (±0.09)	−10.01 (±0.31)	−17.04 (±0.08)	−18.65 (±0.09)
200	—	—	−16.64 (±0.19)	−17.62 (±0.11)
225	−10.65 (±0.03)	−9.38 (±0.25)	−15.59 (±0.26)	−17.01 (±0.04)
265	—	—	−14.95 (±0.12)	−15.97 (±0.25)
275	−10.33 (±0.04)	—	—	—
300	−10.28 (±0.02)	—	—	—

Note: Uncertainties are ±1σ for all data collected at each T.

T range 25–300 °C. Non-linearity of solubility products with $1/T$ is common in heterogeneous reactions between solids and aqueous solutions because of the substantial temperature-dependent decrease of the dielectric constant of H_2O with increasing T and the consequent effect on the thermodynamic properties of aqueous species. The log K values in this paper are derived from the average of all log Q values determined at each T. The average log Q values were fit to a function for variable enthalpy and variable heat capacity to model the T dependence following Plummer and Busenberg (1982):

$$\log K = A + BT + C/T + D \log T. \quad (6)$$

The regression coefficients and their standard errors are summarized in Table 4 and the fit of Equation 6 to the experimental values of log Q is shown graphically in Figure 2. The log Q values above 100 °C, bracketed from undersaturation and from supersaturation, are more reliable than those determined only from undersaturation. Therefore, in some cases the 25 °C experimental data were excluded from the regression analysis, or solubility data were used only from experiments lasting >4000 h. The deviation between the calculated values and the experimental values is generally within ±0.20 log units for analcime and ±0.40 log units for clinoptilolite.

Based on Equation 6 and its first and second derivatives with respect to T, the equations for the standard free energy, enthalpy, entropy, and heat capacity are, respectively:

$$\Delta G_r^0 = -\alpha RT \log K$$
$$= -\alpha R(AT + BT^2 + C + DT \log T) \quad (7)$$
$$\Delta H_r^0 = RT^2(\mathrm{d}\ln K/\mathrm{d}T) = \alpha R(BT^2 - C + DT/\alpha) \quad (8)$$
$$\Delta S_r^0 = -(\Delta G_r^0 - \Delta H_r^0)/T \quad (9)$$
$$\Delta C_p^0 = \partial \Delta H_r^0/\partial T = \alpha R(2BT + D/\alpha) \quad (10)$$

where α is $\ln_e(10) \cong 2.3026$, R is the gas constant (8.3141 J/(mol·K), and T is in kelvins. Calculated values of log K, ΔG_r^0, ΔH_r^0, and ΔS_r^0 at 25 °C and 1 bar are summarized in Table 5 for the Mont St. Hilaire analcime, Wikieup analcime, and the Na- and K-clinoptilolite.

Examples of the time-dependence of the isothermal solubilities approached from undersaturated and supersaturated conditions are shown in Figure 3 for the Mont St. Hilaire analcime at 175 °C and the Na-clinoptilolite at 125 °C. The reversible trends in Figure 3 clearly show that the measured concentrations of ΣAl, ΣNa, and ΣSi represent the steady state solubility of the respective zeolites at each T. The rapid approach to equilibrium evident in Figure 3 is in part caused by the high solid/liquid ratio employed in this study, i.e., the reactive surface area at which dissolution and precipitation may occur is relatively large. However, the measured concentrations of ΣAl, ΣNa, and ΣSi from the Na-clinoptilolite solubility experiments indicate that the solutions are supersaturated with respect to other silica, aluminosilicate, and sodium-

TABLE 4. T dependence of zeolite solubility products

Mineral	A	Standard error	B	Standard error	C	Standard error	D	Standard error
Analcime (Si/Al = 2.0)								
Mont St. Hilaire	224.898	5.863	0.026	0.002	−13 609.700	416.584	−82.060	4.100
Analcime (Si/Al = 2.5)								
Wikieup	224.489	4.122	0.029	0.002	−13 420.200	472.313	−82.105	3.772
Na-clinoptilolite								
(Si/Al = 4.5)	745.150	9.775	0.100	0.007	−38 200.428	1213.920	−272.100	17.952
K-clinoptilolite								
(Si/Al = 4.5)	741.850	10.360	0.103	0.008	−37 980.452	1135.200	−272.088	19.570

Note: log $K = A + BT + C/T + D \log T$, where T is in kelvins. Standard errors obtained from regression analysis.

TABLE 5. Thermodynamic properties of the solubility reactions of analcime and clinoptilolite at 25 °C and 1 bar

Mineral	log K	ΔG_r^0	ΔH_r^0	ΔS_r^0
Alacime				
(Si/Al = 2.0)	−16.06	91.6 ± 2.9	101 ± 30	31.5 ± 4
Analcime				
(Si/Al = 2.5)	−15.05	85.9 ± 2.9	103 ± 30	57.4 ± 4
Na-clinoptilolite				
(Si/Al = 4.5)	−26.47	151.0 ± 2.9	227 ± 30	255.0 ± 4
K-clinoptilolite				
(Si/Al = 4.5)	−28.11	160.4 ± 2.9	228 ± 30	226.8 ± 4

Note: Calculated from regression coefficients in Table 4 and Equations 6–9. Units are kJ/mol for ΔG_r^0 and ΔH_r^0, and J/(mol·K) for ΔS_r^0. Uncertainties are based on estimated errors of ±0.50 log K at 25 °C.

FIGURE 3. Isothermal, time-dependent ion activity products of (**a**) Mont St. Hilaire analcime at 175 °C and (**b**) Castle Creek Na-clinoptilolite at 125 °C. Error bars on log Q values are estimated based on analytical uncertainty.

aluminosilicate phases. For example, with respect to the Mont St. Hilaire analcime, the saturation indices (SI) of solutions in apparent equilibrium with Na-clinoptilolite can be computed as follows:

$$SI = a_{Na^+} a_{Al(OH)_4^-} a_{Si(OH)_4}^2 / K_1 \qquad (11)$$

where a_i is the activity of the respective aqueous species, i, and K_1 is the solubility product of stoichiometric analcime. Values of SI calculated from Equation 11 range from 3 to 25 and tend to increase with increasing T. Furthermore, the solutions in the clinoptilolite experiments were always supersaturated with respect to both quartz and cristobalite. Yet SEM examination and XRD analyses of the clinoptilolite after each experiment indicated that these phases did not precipitate during the solubility experiments, apparently because the concentration of silica required for homogeneous nucleation was not exceeded and the necessary seeds for the growth of cristobalite were not present (Renders et al. 1995). As T increases, the frequency of homogeneous nucleation is expected to increase (Nielsen 1964), an assumption confirmed in an experiment where Na-clinoptilolite and H_2O were heated to 300 °C. In this experiment, because of the high concentrations of silica generated by the dissolving clinoptilolite, quartz nucleation and growth occurred along the liquid-vapor interface in the sealed autoclave; thus, the maximum T was about 265 °C, at which the solubility of clinoptilolite could be determined without the obvious formation of secondary silica phases.

Examination of the data tabulated in the Appendices reveals that the molar ratios of $\Sigma Si/\Sigma Al$ and $\Sigma Na/\Sigma Al$ in solution are generally elevated with respect to the stoichiometric values in the solids. This suggests that precipitation of a secondary aluminous phase occurred during the solubility experiments. Although XRD patterns of the solid materials after the experiments indicate the presence of only analcime or clinoptilolite, this method may not be sufficiently sensitive to detect minute quantities of other possible secondary products. On the other hand, it is also possible that initial dissolution of a trace impurity silica phase in the original Castle Creek clinoptilolite accounts for the elevated molar $\Sigma Si/\Sigma Al$ ratio in the clinoptilolite experiments. In either case, the non-stoichiomet-
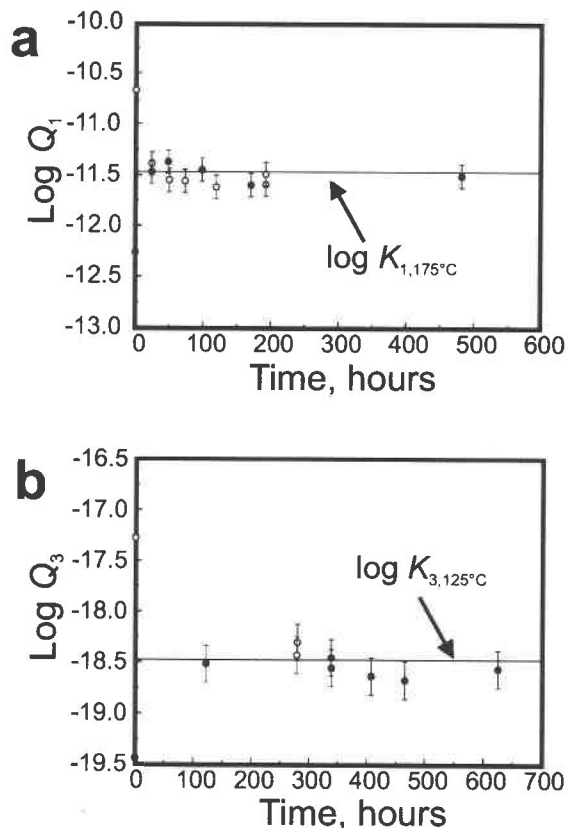
ric ratios in the aqueous solutions complicate unambiguous solubility determinations. The dissolution and precipitation of primary impurities or secondary precipitates of aluminum or silica phases will affect the ratios of elements in solution. These phases, however, may act as buffers of aqueous Si or Al in the same way the silica tubes control aqueous silica concentrations in the sealed silica tube experiments. Furthermore, the solubility constants reported here are in good agreement with corresponding equilibrium constants determined from rate measurements of stoichiometric dissolution and precipitation determined in a flow-through hydrothermal reactor (Wilkin and Barnes 1997). Thus, the reversible, steady-state solubility products for analcime and clinoptilolite shown in Figures 2 and 3 are used to extract standard thermodynamic constants.

Derivation of thermodynamic constants

The solubility products obtained from Equation 6 may be used to calculate standard free energies of formation as a function of T. For the Mont St. Hilaire analcime:

$$\Delta G_r^0 = -\alpha RT \log K_1 \qquad (12)$$

thus, following reaction 1:

TABLE 6. Standard-state Gibbs free energies of formation (kJ/mol) of aqueous species and Gibbs free energies of formation of zeolites derived from regressed values of log K (Table 4)

T (°C)	Na^+ (1)	K^+ (1)	$Al(OH)_4^-$ (2)	$Si(OH)_4$ (3)	$H_2O_{(l)}$ (4)	Mont St. Hilaire analcime	Wikieup analcime	Castle Creek Na-cpt.	Castle Creek Na-cpt.
25	−261.9	−280.0	−1306.1	−1307.8	−237.2	−3089.2	−3044.4	−6267.9	−6107.4
50	−263.4	−285.1	−1309.0	−1313.2	−239.1	−3094.5	−3049.2	−6277.7	−6120.4
90	−266.1	−289.2	−1313.8	−1323.2	−242.3	−3106.7	−3060.6	−6303.4	−6145.9
100	−266.7	−290.2	−1315.1	−1323.8	−243.1	−3106.2	−3059.6	−6031.1	−6143.6
125	−268.5	−292.9	−1318.5	−1329.7	−245.3	−3113.6	−3066.3	−6316.8	−6159.0
175	−272.3	−298.2	−1325.9	−1342.3	−250.1	−3130.1	−3081.0	−6353.0	−6193.7
200	−274.2	−300.8	−1329.7	−1349.0	−252.7	−3138.7	−3088.8	−6372.6	−6212.3
225	−276.2	−303.5	−1333.6	−1355.9	−255.4	−3147.7	−3096.8	−6393.2	−6231.7
265	−279.5	−307.7	−1339.7	−1367.1	−259.8	−3162.6	−3110.0	−6427.2	−6263.2
275	−280.3	−308.8	−1341.1	−1369.6	−261.0	−3165.1	−3112.0	−6433.3	−6268.6
300	−282.3	−311.4	−1344.4	−1378.2	−263.9	−3176.5	−3122.6	−6460.8	−6294.5

Note: (1) Tanger and Helgeson (1988); (2) Diakonov et al. (1996); (3) Walther and Helgeson (1977); (4) Helgeson and Kirham (1974). Gibbs free energies for Na- and K-clinoptilolite were obtained by assuming a constant H_2O content (see text).

$$\Delta G_{f,an}^0 = \Delta G_{f,Na^+}^0 + \Delta G_{f,Al(OH)_4^-}^0 + 2\Delta G_{f,Si(OH)_4}^0$$

$$- \Delta G_r^0 - 5\Delta G_{f,H_2O}^0. \qquad (13)$$

Values for ΔG_f^0 of liquid H_2O, Na^+, and $Si(OH)_4$ at temperatures and pressures along the liquid-vapor equilibrium for the system H_2O were taken from Helgeson and Kirkham (1974), Tanger and Helgeson (1988), and Walther and Helgeson (1977), respectively. The Gibbs free energy of the aluminate ion $Al(OH)_4^-$ was computed as a function of T by using the modified HKF equation of state (Helgeson et al. 1981) and the fitting parameters from Diakonov et al. (1996). These parameters are based, in part, on the T- and pH-dependent solubilities of gibbsite and boehmite (e.g., Wesolowski 1992; Bourcier et al. 1993; Castet et al. 1993). The standard Gibbs free energies of formation of liquid H_2O and the aqueous species used in this study are given in Table 6. The free energies of formation of the zeolites listed in Table 6 were calculated following Equations 12 and 13 by using the tem-

TABLE 7. Hydration numbers (n) and corresponding Gibbs free energies of formation (kJ/mol) of clinoptilolite along the boiling curve of H_2O

	Na-cpt.		K-cpt.	
T (°C)	n	ΔG_f^0	n	ΔG_f^0
25	3.48	−6267.9	2.65	−6107.4
50	3.09	−6179.1	2.37	−6041.6
90	2.58	−6081.5	2.01	−5977.5
100	2.48	−6053.0	1.93	−5955.9
125	2.25	−6010.0	1.76	−5927.3
175	1.90	−5953.3	1.49	−5889.8
200	1.77	−5936.0	1.38	−5878.3
225	1.66	−5924.0	1.28	−5870.2
265	1.51	−5911.2	1.15	−5860.4
275	1.48	−5905.8	1.12	−5855.5
300	1.39	−5904.4	1.03	−5854.8

Note: Hydration numbers correspond to the number of moles of H_2O per $\frac{1}{6}$ of a formula unit. Gibbs free energies were obtained using the thermodynamic data for aqueous species in Table 6 and Equations 12 and 13 adjusted for variable hydration numbers, i.e., $Na_{1.1}Al_{1.1}Si_{4.9} \cdot nH_2O + (12 - n)H_2O = 1.1Na^+ + 1.1Al(OH)_4^- + 4.9Si(OH)_4$.

perature-dependent log K values determined from Equation 6 and the coefficients in Table 4.

For the analcime free energy calculations, it was assumed that the hydration number remains constant along the liquid-vapor equilibrium curve of H_2O. A similar, constant hydration model for clinoptilolite, however, is less reliable (see Carey and Bish 1996). Experimental measurements of the hydration state of the Castle Creek clinoptilolite as a function of T and H_2O vapor P are presented and treated separately in Wilkin (unpublished manuscript, 1998), because of the importance of hydration H_2O to the bulk thermodynamic properties of clinoptilolite and to evaluations of metastable phase equilibria involving clinoptilolite. Here we tabulate standard Gibbs free energies of formation of hypothetical, fully hydrated compositions of Na- and K-clinoptilolite (Table 6). The values in Table 6 were calculated assuming that the stoichiometry of reactions 3 and 4 is independent of T. In addition, hydration states of Na- and K-clinoptilolite at temperatures and pressures along the boiling curve of H_2O and the corresponding Gibbs free energies of formation are given in Table 7. Experimental methods for measuring hydration states at high temperatures and pressures, experimental results, and derived thermodynamic constants for clinoptilolite hydration will be presented in a forthcoming paper. However, note here that clinoptilolite undergoes significant dehydration along the boiling curve of H_2O and that this relative dehydration has a large impact on the standard Gibbs free energies of formation.

The uncertainty in the calculation of free energies using the solubility method is dominated by possible error in the measurement of the reaction free energy. Errors in the log K values include experimental error (± 0.10 log units), uncertainty in activity coefficients (± 0.05 log units), and fitting error (± 0.35 log units), for a total uncertainty of ± 0.50 log units. An uncertainty of 0.50 log units in the measured log K values corresponds to about ± 3 and ± 11 kJ/mol at 25 and 300 °C, respectively. A total of 5–10 kJ/mol is considered to be a reasonable
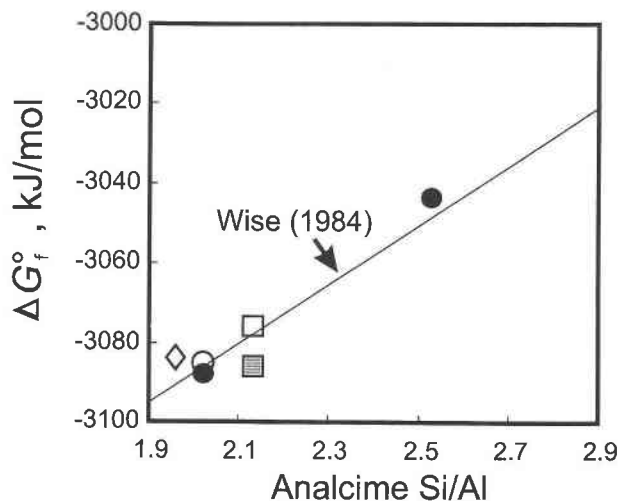
FIGURE 4. Standard Gibbs free energy of formation of analcime at 25 °C vs. Si-Al (open diamond, Murphy et al. 1996; open circle, Helgeson et al. 1978; open square, Johnson et al. 1982; shaded square, Johnson et al. 1992; and filled circles, this study). Also plotted is the ideal solid solution model of Wise (1984).

estimate of error on the calculated standard free energies of formation given in Tables 6 and 7.

Analcime

Calculated ΔG_f^0 values of analcime are given to 300 °C in Table 6. The free energy value at 25 °C and 1 bar of the Si-rich analcime from Wikieup (-3044.4 kJ/mol) is about 45 kJ/mol greater than that of the stoichiometric Mont St. Hilaire analcime. The standard Gibbs free energy of the Mont St. Hilaire analcime at 25 °C (-3089.2 kJ/mol) agrees favorably with the value of -3088.2 kJ/mol reported by Helgeson et al. (1978). They derived thermodynamic data for stoichiometric analcime from the results of unpublished hydrothermal experiments (J. Hemly, U.S. Geological Survey) in which concentrations of aqueous silica were measured for aqueous solutions coexisting with the mineral assemblage analcime+albite. Based on adiabatic, solution, and drop-calorimetric techniques, Johnson et al. (1982) reported a value of ΔG_f^0 of -3077.2 ± 3.3 kJ/mol at 25 °C and 1 bar for analcime with the composition $Na_{0.96}Al_{0.96}Si_{2.04}O_6 \cdot H_2O$. This free energy, however, was subsequently revised in Johnson et al. (1992) to account for changes in base reactions for SiO_2 and the enthalpy of formation of gibbsite; the revised value reported was -3086.1 kJ/mol. Recently, Murphy et al. (1996) reported the results of low-temperature (25 °C) solubility experiments and estimated a ΔG_f^0 value of -3085.4 kJ/mol for an Al-enriched analcime (Si/Al = 1.94) from Mont St. Hilaire, Quebec.

The standard state ΔG_f^0 values of the respective analcimes noted above are plotted in Figure 4 against their corresponding Si/Al ratios. Although there is some scatter, the free energy values generally follow the linear relationship suggested by Wise (1984)

$$\Delta G_{f,anss}^0 = -3088.1 + 74.3 \cdot (Si/Al - 2) \qquad (14)$$

where $\Delta G_{f,anss}^0$ is the standard free energy in kJ/mol of an analcime with variable Si-Al. Discrepancies in the measured thermodynamic properties of analcime may be caused by factors such as variable states of strain in starting materials (e.g., Liu et al. 1995) and differences in configurational entropies from Si-Al ordering (e.g., Phillips and Kirkpatrick 1994; Kiseleva et al. 1996a).

The free energies of analcime can be used to test thermodynamic models approximating properties such as ΔG_f^0 and ΔH_f^0 (La Iglesia and Aznar 1986). These empirical models are based upon the addition of ΔG_f^0 or ΔH_f^0 of the constituent oxides and, therefore, ignore contributions from disorder in the Al,Si-tetrahedra comprising zeolite frameworks. The model of La Iglesia and Aznar (1986) predicts values of -3085.6 and -3043.5 kJ/mol for analcime with Si/Al ratios of 2.0 and 2.5, respectively. Both of these values are larger but within 0.12% of the experimental values determined here.

Clinoptilolite

Gibbs free energies of hydrous Na- and K-clinoptilolite are listed in Table 7. The ΔG_f^0 values are -6267.9 and -6107.4 kJ/mol at 25 °C and 1 bar for fully hydrated Na- and K-clinoptilolite, respectively.

Thermodynamic properties of two natural clinoptilolites determined by calorimetry were reported in Hemingway and Robie (1984) and Johnson et al. (1991). Bowers and Burns (1990) used the heat-capacity and entropy data of Hemingway and Robie (1984) to estimate a ΔG_f^0 of -6316 ± 38 kJ/mol at 25 °C and 1 bar for clinoptilolite with the composition $Na_{0.09}K_{0.16}Ca_{0.25}Mg_{0.21}Al_{1.11}Si_{4.83}$-$O_{12} \cdot 3.67H_2O$. Johnson et al. (1991) made calorimetric measurements on clinoptilolite crystals from Malheur County, Oregon with the composition $Na_{0.32}K_{0.18}Ca_{0.25}$-$Mg_{0.04}Al_{1.15}Si_{4.84}O_{12} \cdot 3.6H_2O$ and found a ΔG_f^0 of -6359.5 kJ/mol at 25 °C. Based on solubility experiments at 25 °C, Murphy et al. (1996) reported a provisional ΔG_f^0 of -6354.0 kJ/mol for a comparatively Si-rich, and idealized Na-clinoptilolite with the composition $NaAlSi_5$-$O_{12} \cdot 4H_2O$. A direct comparison between the values presented here for Na- and K-clinoptilolite and the values reported by Bowers and Burns (1990), Johnson et al. (1991), and Murphy et al. (1996) is complicated by differences among the various clinoptilolites in the exchangeable cation composition, Si/Al ratio, and H_2O content.

To evaluate the Si-Al effect on the thermochemical properties of clinoptilolite, anhydrous free energies of formation of the above clinoptilolites are plotted in Figure 5 against their corresponding Si/Al ratios. The anhydrous free energies of formation are calculated assuming that each H_2O molecule in the clinoptilolite framework contributes -255.8 kJ/mol to the total free energy at 25 °C (see Johnson et al. 1991). Apparently, the anhydrous clinoptilolite framework becomes more stable with increasing Al content, in agreement with the calorimetric work
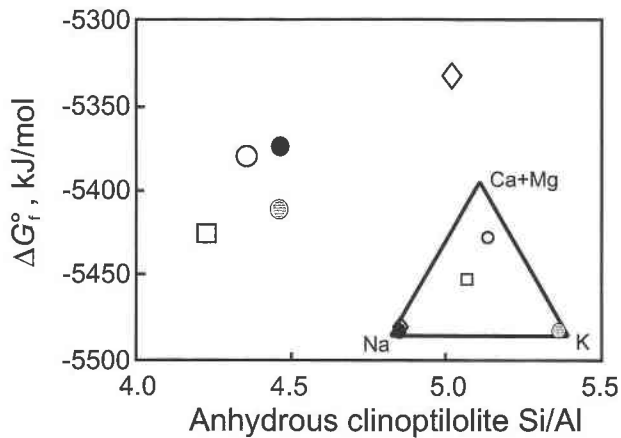
FIGURE 5. Standard Gibbs free energy of formation of anhydrous clinoptilolite at 25 °C vs. Si-Al (open square, Bowers and Burns 1990; open circle, Johnson et al. 1991; open diamond, Murphy et al. 1996; filled circle, this study, Na-clinoptilolite; and shaded circle, this study, K-clinoptilolite). The ternary diagram indicates the negative proportions of Na, K, and Ca + Mg in clinoptilolites for which the thermodynamic data were reported.

on Na-faujasite by Petrovic and Navrotsky (1997). The latter authors found a negative, linear dependence of ΔH_f^0 of dehydrated faujasite on the Si/Al ratio, implying a stabilizing exothermic enthalpy of the charge-coupled substitution, $Si^{4+} \rightarrow Al^{3+} + Na^+$.

The solid-solution behavior of clinoptilolite along the Na-K join may be described by the reaction:

$$Na_xK_{1-x}\text{-clinoptilolite(ss)} + yK^+$$

$$= K_{1-x+y}Na_{x-y}\text{-clinoptilolite} + yNa^+. \quad (15)$$
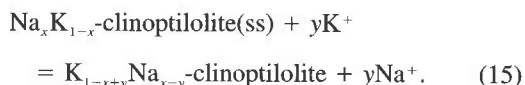
The standard distribution coefficient, K_D, defining reaction 15 is

$$K_D = (a_{Na^+}^y/a_{K^+}^y)(a_{K-Cpt(ss)}) = K_{Na-Cpt}/K_{K-Cpt}. \quad (16)$$
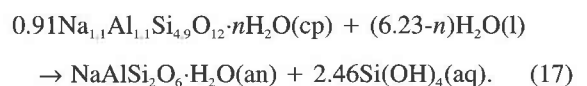
The distribution coefficient corresponds to the quotient of the solubility product for the end-member Na- and K-clinoptilolites; at 25 °C, $K_D = 31.0$ based on an exchange of 1.0 cations. For a clinoptilolite mixture of composition 0.5 Na-clinoptilolite + 0.5 K-clinoptilolite, and assuming ideal behavior in both the solid and the aqueous solution, at equilibrium the fluid should be enriched by about 30× in Na^+ over K^+. These data are consistent with the selectivity for K over Na that clinoptilolite exhibits in ion exchange studies (e.g., Pabalan 1994). For example, Pabalan (1994) determined the log K_{ex} for Na-K exchange in clinoptilolite to be 1.40 ± 0.01; the corresponding value of the Gibbs free energy of exchange is 7.98 ± 0.08 kJ/mol. The values for log K_{ex} and ΔG_{ex}^0 determined here are 1.49 ± 0.50 and 8.52 ± 2.85 kJ/mol. Values of log K_{ex} exhibit a slight, monotonic decrease with increasing T, at 200 °C, log $K_{ex} = 1.26 \pm 0.50$.

Geologic implications

To assess the stability limits of clinoptilolite in aqueous solutions and to consider possible diagenetic transformations of clinoptilolite due to changing water chemistry, Bowers and Burns (1990) constructed activity diagrams using measured and estimated thermodynamic data for silicate minerals, aqueous species, and H_2O in the multi-component system, $Na_2O-K_2O-CaO-MgO-Fe_2O_3-Al_2O_3-SiO_2-H_2O$. An important conclusion of their study was that clinoptilolite formation and persistence is favored only when aqueous silica activities exceed those of equilibrium quartz solubility. Consequently, the common natural association of clinoptilolite with opal-CT is consistent with the calculated wide metastability field of clinoptilolite in solutions saturated with cristobalite or amorphous silica. The solubility data presented here also show that the concentrations of silica generated by dissolving clinoptilolite were typically between cristobalite and amorphous silica-saturation. These high silica concentrations were most apparent in experiments at T greater than 265 °C where silica concentrations promoted quartz nucleation along the liquid-vapor interface in the sealed autoclave. Therefore, the persistence of clinoptilolite may depend on the absence of quartz nucleation and growth. However, as discussed below, clinoptilolite may be stabilized in quartz-saturated solutions if the activities of aqueous cations and/or Al are high enough to compensate for a low silica activity.

The spatial distribution of clinoptilolite and analcime in sedimentary and volcanic-hosted occurrences implies that analcime is produced by replacement of earlier-formed zeolites including clinoptilolite (e.g., Hay 1966; Sheppard and Gude 1969; Bish and Aronson 1993). Based on microanalytical techniques, Sheppard and Gude (1969) suggested that high-Si analcimes form by replacement reactions of high-Si precursor zeolites, such as clinoptilolite and erionite, whereas low-Si analcimes form by replacement of low-Si zeolite precursors, such as phillipsite. In an experimental study, Boles (1971) also found a strong correlation between the Si/Al of precursor clinoptilolites and the Si/Al in synthetic analcimes. The mechanisms of replacement among zeolites are, at present, equivocal, and both dissolution-precipitation and solid-state reaction paths have been proposed.

As part of a modeling study on water-rock interactions at Yucca Mountain, Kerrisk (1983) concluded that the clinoptilolite-to-analcime transition is controlled by the activity of silica, and analcime formation is favored at silica activities equivalent to quartz saturation. The effect of dissolved Si on the clinoptilolite-to-analcime reaction may be evaluated by considering the reaction between Na-clinoptilolite and stoichiometric analcime:

$$0.91Na_{1.1}Al_{1.1}Si_{4.9}O_{12} \cdot nH_2O(cp) + (6.23-n)H_2O(l)$$

$$\rightarrow NaAlSi_2O_6 \cdot H_2O(an) + 2.46Si(OH)_4(aq). \quad (17)$$

In dilute aqueous solutions with H_2O activity close to unity, the equilibrium constant of reaction 17 is equiva-
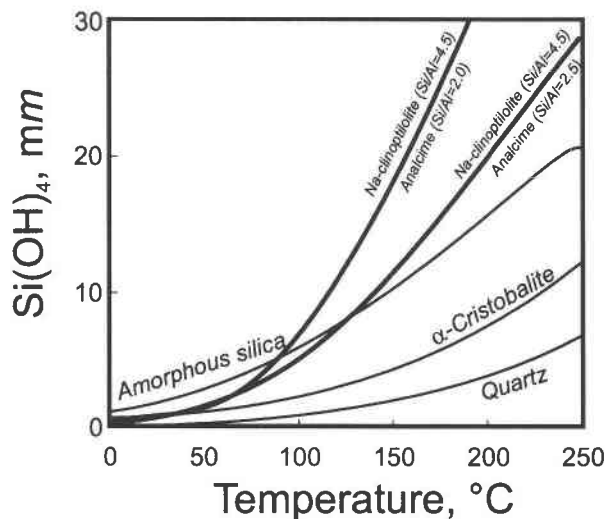
FIGURE 6. Temperature-dependent silica concentration marking the boundary between the stability fields of analcime and Na-clinoptilolite compared to the solubilities of amorphous silica, α-crisobalite, and quartz (assuming silica activity and concentration are equivalent; see text).

FIGURE 7. Stability relations between clinoptilolite and analcime at 175 °C (see text for discussion).

lent to an activity of $Si(OH)_4$ at which clinoptilolite and analcime are in metastable equilibrium:

$$\log K_{17} = 0.91 \log K_3 - \log K_1 = 2.46 \log a_{Si(OH)_4}. \quad (18)$$

The equilibrium constant defined in Equation 18 has been calculated as a function of T using Equation 6 and the regression coefficients listed in Table 4 for $\log K_1$ and $\log K_3$. The critical activity of aqueous silica, separating the equilibrium fields of Na-clinoptilolite and analcime, is plotted in Figure 6 as a function of T and compared to the solubilities of quartz, α-cristobalite, and amorphous silica.

Based on a metastable equilibrium model, if the solubility of amorphous silica is taken as the maximum possible silica concentration in solution, the curves in Figure 6 indicate that Na-clinoptilolite should not persist above ~90 °C. At cristobalite saturation, Na-clinoptilolite should not persist above ~50 °C. The fact that clinoptilolite does persist to T ~175 °C (Kristmannsdottir and Tomasson 1978; Bish and Aronson 1993) suggests that the reaction of Na-clinoptilolite to analcime is controlled kinetically. At cristobalite saturation, the deviation between the univariant curve and the curve showing cristobalite solubility in Figure 6 is a measure of the affinity of the replacement reaction (Eq. 17). The reaction affinity increases rapidly at T above ~100 °C; thus, it is expected that the rate of conversion would also increase rapidly above this T. The apparent control of aqueous silica concentration on the conversion, i.e., dropping from amorphous silica- to quartz-saturated concentrations may be related more to an increase in reaction affinity rather than to an equilibrium control on the reaction. Note that the replacement of Na-clinoptilolite with Si/Al = 4.50 by analcime with a Si/Al = 2.55 shifts the equilibria to
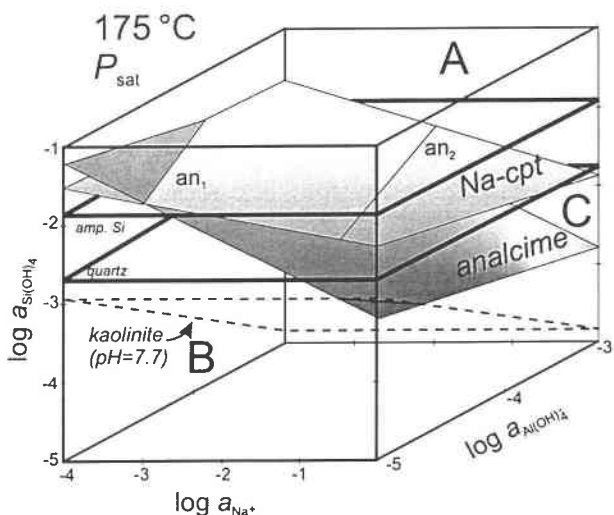
slightly lower silica activities at any given T, thus expanding the stability field of clinoptilolite and decreasing the overall affinity of reaction 17 at any given T.

The isothermal, aqueous solubilities of three-component zeolites may be represented on $\log a_{Si(OH)_4} - \log a_{Na^+} - \log a_{Al(OH)_4^-}$ diagrams. In Figure 7, fluids with compositions plotting above the solubility planes (region A) are supersaturated with respect to both analcime and clinoptilolite and those plotting below both planes (region B) are undersaturated. Note that for the conditions considered in Figure 7, solutions saturated in Na-clinoptilolite are supersaturated in kaolinite as well as several other aluminosilicate and sodium-aluminosilicate minerals. The zeolite planes intersect along a line (e.g., an_1) that defines fluid compositions in metastable equilibrium with clinoptilolite and analcime. At 175 °C, this line corresponds to aqueous Si activities exceeding amorphous silica saturation; consequently, it is unlikely that clinoptilolite and analcime are ever in metastable equilibrium above 175 °C. Below 175 °C, the intersection of the solubility planes, however, does move into the compositional space between quartz and amorphous silica saturation. The intersection is marked schematically (an_2) in Figure 7 between the solubility plane of the Na-clinoptilolite and that of the Si-rich Wikieup analcime. Again the stability field of clinoptilolite is expanded by considering equilibria with more silica-enriched analcime compositions. On the other hand, decreasing the clinoptilolite Si/Al ratio should have the effect of narrowing the stability field of clinoptilolite relative to the range of possible analcime compositions.

Fluid compositions in region C are undersaturated in Na-clinoptilolite and supersaturated in analcime, and it is there that replacement of clinoptilolite by analcime should occur. Note that a fluid saturated with clinoptilolite could move into region C if the activities were decreased of any, or all, components Na^+, $Al(OH)_4^-$, and $Si(OH)_4$.
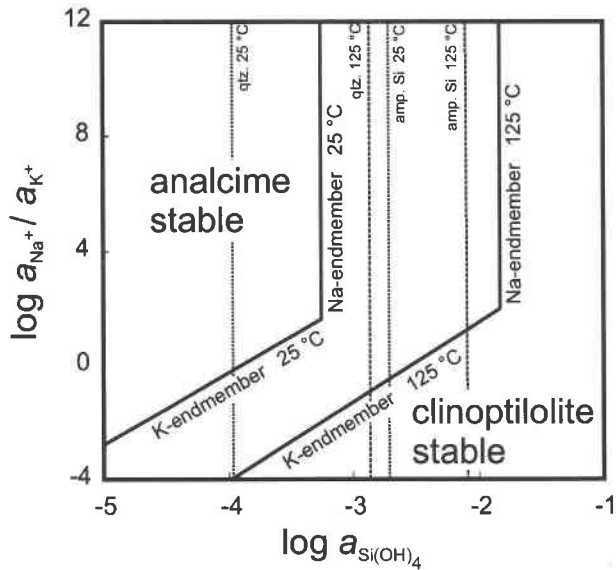
FIGURE 8. Activity diagram showing stability relations of Na-clinoptilolite, K-clinoptilolite, and analcime.

Thus, although a decrease in silica activity by the nucleation and growth of quartz is an efficient mechanism of driving this zeolite transformation (Bowers and Burns 1990), decreasing the activity of aluminate, silica, or sodium ions (for example, by fluid mixing and dilution) could also be important.

The effect of cation composition on the clinoptilolite-analcime equilibria is evaluated in Figure 8. The activity diagram (Fig. 8) was constructed with the approximation of ideal mixing in clinoptilolite and Al conservation in the solid phases. Both Na-clinoptilolite and K-clinoptilolite are stable at 25 °C relative to stoichiometric analcime in amorphous silica-saturated solutions. In quartz-saturated solutions at 25 °C, Na-clinoptilolite is unstable relative to stoichiometric analcime; however, K-clinoptilolite is stable in solutions with $a_{Na^+}/a_{K^+} < 0.59$. At 125 °C, Na-clinoptilolite is unstable even at amorphous silica-saturation, but K-clinoptilolite can be stable at aqueous silica activities between quartz and amorphous silica-saturation depending on a_{Na^+}/a_{K^+}. Figure 8 clearly illustrates how potassic compositions of clinoptilolite can be stabilized relative to sodic compositions depending on solution composition.

ACKNOWLEDGMENTS

REFERENCES CITED

Armbruster, T. and Gunter, M.E. (1991) Stepwise dehydration of heuland-ite-clinoptilolite from Succor Creek, Oregon, U.S.A.: A single-crystal X-ray study at 100 K. American Mineralogist, 76, 1872–1883.

Barnes, H.L. (1971) Investigations in hydrothermal sulfide systems. In G.C. Ulmer, Ed., Research techniques for high pressure and high temperature, p. 317–355. Springer-Verlag, New York.

Bish, D.L. (1984) Effects of exchangeable cation composition on the thermal expansion/contraction of clinoptilolite. Clays and Clay Minerals, 32, 444–452.

———(1988) Effects of composition on the dehydration behavior of clinoptilolite and heulandite. In D. Kalló and H. Sherry, Eds., Occurrence, properties and utilization of natural zeolites, p. 565–576. Akadémiai Kiadoó, Budapest.

Bish, D.L. and Aronson, J.L. (1993) Paleogeothermal and paleohydrologic conditions in silicic tuff from Yucca Mountain, Nevada. Clays and Clay Minerals, 41, 148–161.

Boles, J.R. (1971) Synthesis of analcime from natural heulandite and clinoptilolite. American Mineralogist, 56, 1724–1734.

———(1972) Composition, optical properties, cell dimensions, and thermal stability of some heulandite group zeolites. American Mineralogist, 57, 1463–1493.

Bourcier, W.L. and Barnes, H.L. (1987) Rocking autoclaves for hydrothermal experiments I. Fixed volume systems. In G.C. Ulmer and H.L. Barnes, Eds., Hydrothermal experimental techniques, p. 189–215. Wiley, New York.

Bourcier, W.L., Knauss, K.G., and Jackson, K.J. (1993) Aluminum hydrolysis constants to 250 °C from boehmite solubility experiments. Geochimica et Cosmochimica Acta, 57, 747–762.

Bowers, T.S. and Burns, R.G. (1990) Activity diagrams for clinoptilolite: Susceptibility of this zeolite to further diagenetic reactions. American Mineralogist, 75, 601–619.

Broxton, D.E., Bish, D.L., and Warren, R.G. (1987) Distribution and chemistry of diagenetic minerals at Yucca Mountain, Nye County, Nevada. Clays and Clay Minerals, 35, 89–110.

Busey, R.H. and Mesmer, R.E. (1977) Ionization equilibria of silicic acid and polysilicate formation in aqueous sodium chloride solutions to 300 °C. Inorganic Chemistry, 16, 2444–2450.

———(1978) Thermodynamic quantities for the ionization of water in sodium chloride media to 300 °C. Journal of Chemical Engineering Data, 23, 175–176.

Carey, J.W. and Bish, D.L. (1996) Equilibrium in the clinoptilolite-H$_2$O system. American Mineralogist, 81, 952–962.

Castet, S., Dandurand, J., Schott, J., and Gout, R. (1993) Boehmite solubility and aqueous aluminum speciation in hydrothermal solutions (908–350 °C): Experimental study and modeling. Geochimica et Cosmochimica Acta, 57, 4869–4884.

Diakonov, I., Pokrovski, G., Schott, J., Castet, S., and Gout, R. (1996) An experimental and computational study of sodium-aluminum complexing in crustal fluids. Geochimica et Cosmochimica Acta, 60, 197–211.

Feng, X. and Savin, S.M. (1993) Oxygen isotope studies of zeolites-Stilbite, analcime,heulandite, and clinoptilolite II. Kinetics and mechanisms of isotopic exchange between zeolites and water vapor. Geochimica et Cosmochimica Acta, 57, 4219–4238.

Gammons, C.H. and Barnes, H.L. (1989) The solubility of Ag$_2$S in near-neutral aqueous sulfide solutions at 25 to 300 °C. Geochimica et Cosmochimica Acta, 53, 279–290.

Gingele, F.X. and Schulz, H.D. (1993) Authigenic zeolites in Late Pleistocene sediments of the South Atlantic (Angola Basin). Marine Geology, 111, 121–131.

Gottardi, G. and Galli, D. (1985) Natural zeolites, 409 p. Springer-Verlag, Berlin.

Gunter, M.E., Armbruster, T., Kohler, T., and Knowles, C.R. (1994) Crystal structure and optical properties of Na- and Pb-exchanged heulandite-group zeolites. American Mineralogist, 79, 675–682.

Hay, R.L. (1966) Zeolites and zeolitic reactions in sedimentary rocks. Geological Society of America Special Paper, 85, 130.

———(1978) Geologic occurrence of zeolites. In L.B. Sand and F.A. Mumpton, Eds., Natural zeolites: Occurrence, properties, use, p. 135–143. Pergamon Press, New York.

Helgeson, H.C. and Kirkham, D.H. (1974) Theoretical prediction of the thermodynamic behavior of aqueous electrolytes at high pressures and temperatures: II. Debye-Hückel parameters for activity coefficients and relative partial-molal properties. American Journal of Science, 274, 1199–1261.

Helgeson, H.C., Delany, J.M., Nesbitt, H.W., and Bird, D.K. (1978) Summary and critique of the thermodynamic properties of rock forming minerals. American Journal of Science, 278A, 1–229.

Helgeson, H.C., Kirkham, D.H., and Flowers, G.C. (1981) Theoretical prediction of the thermodynamic behavior of aqueous electrolytes at high pressures and temperatures: IV. Calculation of activity coefficients, osmotic coefficients, and apparent molal and standard and relative partial molal properties to 600 °C and 5 kb. American Journal of Science, 281, 1249–1516.

Hemingway, B.S. and Robie, R.A. (1984) Thermodynamic properties of zeolites: low-temperature heat capacities and thermodynamic functions of phillipsite and clinoptilolite. Estimates of the thermochemical properties of zeolitic water at low temperatures. American Mineralogist, 69, 692–700.

Howell, D.A., Johnson, G.K., Tasker, I.R., O'Hare, P.A.G., and Wise, W.S. (1990) Thermodynamic properties of the zeolite stilbite. Zeolites, 10, 525–531.

Iijima, A. and Utada, M. (1966) Zeolites in sedimentary rocks, with reference to the depositional environments and zonal distribution. Sedimentology, 7, 327–357.

Johnson, G.K., Flotow, H.E., O'Hare, P.A.G., and Wise, W.S. (1982) Thermodynamic studies of zeolites: analcime and dehydrated analcime. American Mineralogist, 67, 736–748.

Johnson, G.K., Flotow, H.E., and O'Hare, P.A.G. (1983) Thermodynamic studies of zeolites: natrolite, mesolite, and scolecite. American Mineralogist, 68, 1134–1145.

————(1985) Thermodynamic studies of zeolites: heulandite. American Mineralogist, 70, 1065–1071.

Johnson, G.K., Tasker, I.R., Jurgens, R., and O'Hare, P.A.G. (1991) Thermodynamic studies of zeolites: clinoptilolite. Journal of Chemical Thermodynamics, 23, 475–484.

Johnson, G.K., Tasker, I.R., Flotow, H.E., O'Hare, P.A.G., and Wise, W.G. (1992) Thermodynamic studies of mordenite, dehydrated mordenite, and gibbsite. American Mineralogist, 77, 85–93.

Kastner, M. and Stonecipher, S.A. (1978) Zeolites in pelagic sediments of the Atlantic, Pacific, and Indian Oceans. In L.B. Sand and F.A. Mumpton, Eds., Natural zeolites: Occurrence, properties, use, p. 199–220. Pergamon Press, New York.

Kerrisk, J.F. (1983) Reaction-path calculations of groundwater chemistry and mineral formation at Rainier Mesa, Nevada. U.S. National Technical Information Service, Report LA-10929.

Kiseleva, I., Navrotsky, A., Belitsky, I.A., and Fursenko, B.A. (1996a) Thermochemistry and phase equilibria in calcium zeolites. American Mineralogist, 81, 658–667.

————(1996b) Thermochemistry of natural potassium sodium calcium leonhardite and its cation-exchanged forms. American Mineralogist, 81, 668–675.

Kristmanndottir, H. and Tomasson, J. (1978) Zeolite zones in geothermal areas of Iceland. In L.B. Sand and F.A. Mumpton, Eds., Natural zeolites: Occurrence, properties, use, p. 277–284. Pergamon Press, New York.

La Iglesia, A. and Aznar, A.J. (1986) A method of estimating the Gibbs energies of formation of zeolites. Zeolites, 6, 26–29.

Liu, M., Yund, R.A., Tullis, J., Topor, L., and Navrotsky, A. (1995) Energy associated with dislocations: a calorimetric study using synthetic quartz. Physics and Chemistry of Minerals, 22, 67–73.

Mondale, K.D., Mumpton, F.A., and Aplan, F.F. (1988) Properties and beneficiation of natural sedimentary zeolites. In D.J.T. Carson and A.H. Vassiliou, Eds., Process mineralogy VIII, p. 249–275. The Minerals, Metals, and Materials Society, Pennsylvania.

Murphy, W.M., Pabalan, R.T., Prikryl, J.D., and Goulet, C.J. (1996) Reaction kinetics and thermodynamics of aqueous dissolution and growth of analcime and Na-clinoptililote at 25°C. American Journal of Science, 296, 128–186.

Nielsen, A.E. (1964) Kinetics of precipitation, 153 p. Pergamon Press, New York.

Noto, M. and Kusakabe, M. (1997) An experimental study of oxygen isotope fractionation between wairakite and water. Geochimica et Cosmochimica Acta, 61, 2083–2093.

Pabalan, R.T. (1994) Thermodynamics of ion exchange between clinoptilolite and aqueous solutions of Na^+/K^+ and Na^+/Ca^{2+}. Geochimica et Cosmochimica Acta, 58, 4573–4590.

Petrovic, I. and Navrotsky, A. (1997) Thermochemistry of Na-faujasites with varying Si/Al ratios. Microporous Materials, 9, 1–12.

Phillips, B.L. and Kirkpatrick, R.J. (1994) Short-range Si-Al order in leucite and analcime: Determination of the configurational entropy from ^{27}Al and variable-temperature ^{29}Si NMR spectroscopy of leucite, its Cs- and Rb-exchanged derivatives, and analcime. American Mineralogist, 79, 1025–1031.

Plummer, N.L. and Busenberg, E. (1982) The solubilities of calcite, aragonite and vaterite in CO_2-H_2O solutions between 0 and 90 °C. Geochimica et Cosmochimica Acta, 46, 1011–1040.

Pokrovskii, V.A. and Helgeson, H.C. (1995) Thermodynamic properties of aqueous species and the solubilities of minerals at high pressures and temperatures: The system Al_2O_3-H_2O-NaCl. American Journal of Science, 295, 1255–1342.

Renders, P.J.N., Gammons, C.H., and Barnes, H.L. (1995) Precipitation and dissolution rate constants for cristobalite from 150 to 300 °C. Geochimica et Cosmochimica Acta, 59, 77–85.

Sheppard, R.A. and Gude, A.J. III (1969) Diagenesis of tuffs in the Barstow Formation, Mud Hills, San Bernardino County, California. U.S. Geological Survey Professional Paper, 597, 38.

Simonot-Grange, M.H. (1979) Thermodynamic and structural features of water sorption in zeolites. Clays and Clay Minerals, 27, 423–428.

Stahl, K., Kvick, A., and Smith, J.V. (1990) Thomsonite: neutron diffraction study at 13 K. Acta Crystallographica, 46, 1370–1373.

Surdam, R.C. and Sheppard, R.A. (1978) Zeolites in saline, alkaline-lake deposits. In L.B. Sand and F.A. Mumpton, Eds., Natural zeolites: Occurrence, properties, use, p. 145–174. Pergamon Press, New York.

Tanger, J.C. and Helgeson, H.C. (1988) Calculation of the thermodynamic and transport properties of aqueous species at high pressures and temperatures: Revised equations of state for the standard partial molal properties of ions and electrolytes. American Journal of Science, 288, 19–98.

Walther, J.V. and Helgeson, H.C. (1977) Calculation of the thermodynamic properties of aqueous silica and the solubility of quartz and its polymorphs at high pressures and temperatures. American Journal of Science, 277, 1315–1351.

Ward, R.L. and McKague, H.L. (1994) Clinoptilolite and heulandite structural differences as revealed by multinuclear magnetic resonance spectroscopy. Journal of Physical Chemistry, 98, 1232–1237.

Wesolowski, D.J. (1992) Aluminum speciation and equilibria in aqueous solution: I. The solubility of gibbsite in the system Na-K-Cl-OH-$Al(OH)_4$ from 0 to 100 °C. Geochimica et Cosmochimica Acta, 56, 1065–1091.

Wesolowski, D.J. and Palmer, D.A. (1994) Aluminum speciation and equilibria in aqueous solution: V. Gibbsite solubility at 50 °C and pH 3-9 in 0.1 molal NaCl solutions (a general model for aluminum speciation; analytical methods). Geochimica et Cosmochimica Acta, 58, 2947–2969.

Wilkin, R.T. and Barnes, H.L. (1997) Temperature and free-energy dependence of zeolite precipitation and dissolution rates (abstracts). Seventh Annual V.M. Goldschmidt Conference, 219. Lunar and Planetary Institute, Houston, U.S.A.

Wise, W.S. (1984) Thermodynamic studies of zeolites: Analcime solid solutions. In D. Olson and A. Bisio, Eds., Proceedings of the sixth international zeolite conference, p. 616–623. Butterworths, Guildford, U.K.

APPENDIX TABLE 1.   Experimental solubility data for analcime and Na-clinoptilolite

Sample	T (°C)	Time (hours)	ΣSi (mm)	ΣAl (mm)	ΣNa (mm)	pH$_{25}$	Direction	log Q_i
				Mont St. Hilaire analcime				
21	90	787	1.20	0.14	0.22	8.28	↑	−13.36
22	90	787	1.11	0.14	0.30	8.28	↑	−13.31
27	125	576	0.88	0.39	2.55	8.70	↑	−12.15
28	125	576	0.85	0.38	2.50	8.70	↑	−12.21
29	125	576	0.84	0.37	2.45	8.70	↑	−12.24
30	175	24	1.52	0.79	2.17	—	↑	−11.45
31	175	48	1.64	0.87	2.14	—	↑	−11.35
32	175	98	1.56	0.82	2.10	—	↑	−11.42
33	175	170	1.46	0.73	1.89	—	↑	−11.42
34	175	482	1.54	0.73	2.23	9.47	↑	−11.58
35	175	482	1.51	0.73	2.25	9.47	↑	−11.48
36	225	119	2.56	1.45	3.16	9.82	↑	−10.62
37	225	119	2.52	1.49	3.16	9.82	↑	−10.62
38	275	98	3.68	1.59	3.29	9.16	↑	−10.29
39	275	98	3.63	1.61	3.31	9.16	↑	−10.29
46	300	35	4.31	1.61	2.39	8.42	↑	−10.29
47	300	35	4.37	1.62	2.49	8.42	↑	−10.26
48	275	47	4.42	1.34	2.24	8.85	↓	−10.36
49	275	47	4.49	1.36	2.27	8.85	↓	−10.33
50	275	47	4.35	1.28	2.21	8.85	↓	−10.40
51	225	52	3.76	0.89	2.17	8.65	↓	−10.66
52	225	52	3.72	0.87	2.07	8.65	↓	−10.69
60	175	24	2.73	0.34	1.96	—	↓	−11.36
61	175	50	2.51	0.29	1.83	—	↓	−11.53
62	175	73	2.50	0.28	1.86	—	↓	−11.54
64	175	119	2.42	0.27	1.86	—	↓	−11.59
67	175	193	2.32	0.27	1.88	8.15	↓	−11.62
68	175	193	2.41	0.30	1.92	8.15	↓	−11.53
71	125	22	2.11	0.20	1.76	—	↓	−11.86
72	125	44	1.95	0.20	1.82	—	↓	−11.89
73	125	92	1.76	0.15	1.77	—	↓	−12.14
76	125	198	1.66	0.11	1.76	7.97	↓	−12.31
77	125	198	1.70	0.11	1.79	7.97	↓	−12.28
78	90	89	1.55	0.07	1.83	7.64	↓	−12.56
83	90	326	1.40	0.04	1.72	7.37	↓	−12.95
84	90	374	1.37	0.04	1.69	7.35	↓	−12.97
86	90	432	1.36	0.04	1.73	7.33	↓	−12.98
B1	25	3288	0.03	0.009	10.4	8.32	↑	−15.99
B2	25	3288	0.02	0.014	11.2	8.32	↑	−16.11
C1	50	2520	0.07	0.032	12.8	7.79	↑	−14.75
C2	50	2520	0.07	0.031	12.8	7.79	↑	−14.72
B10	25	1020	0.016	0.008	9.3	7.89	↑	−16.76
B11	25	1020	0.027	0.008	9.5	7.89	↑	−16.31
B12	25	4125	0.026	0.012	10.5	8.01	↑	−16.12
B13	25	4125	0.031	0.012	11.2	8.01	↑	−15.94
C10	50	4125	0.075	0.019	9.8	8.05	↑	−15.01
C11	50	4125	0.108	0.027	10.0	8.05	↑	−14.52
				Wikieup analcime				
108	125	196	3.24	0.12	1.32	9.15	↑	−11.34
109	125	196	3.28	0.12	1.30	9.15	↑	−11.33
114	175	93	7.61	0.19	1.39	8.82	↑	−10.28
115	175	93	7.68	0.19	1.36	8.82	↑	−10.28
116	225	48	14.56	0.33	2.06	8.95	↑	−9.38
117	225	48	14.66	0.33	2.05	8.95	↑	−9.38
123	175	49	13.65	0.16	2.38	8.87	↓	−9.65
124	175	49	13.71	0.16	2.39	8.87	↓	−9.62
127	125	117	10.56	0.02	1.86	8.88	↓	−10.75
128	125	117	10.77	0.03	1.85	8.88	↓	−10.69
131	90	483	4.78	0.005	1.43	8.80	↓	−12.09
132	90	483	4.55	0.005	1.36	8.80	↓	−12.10
150	125	403	3.00	0.36	1.30	9.26	↑	−11.13
151	125	403	3.20	0.38	1.40	9.26	↑	−11.03
157	175	174	8.07	0.23	1.50	9.28	↑	−10.21
158	90	556	1.87	0.02	1.14	8.82	↑	−12.53
B3	25	3288	0.050	0.004	10.0	8.33	↑	−15.58
B4	25	3288	0.045	0.004	10.0	8.33	↑	−15.68
B5	25	3288	0.056	0.004	9.7	8.33	↑	−15.48
C3	50	2520	0.177	0.008	11.8	7.65	↑	−14.07
C4	50	2520	0.168	0.012	12.1	7.65	↑	−13.97
C5	50	2520	0.153	0.008	11.5	7.65	↑	−14.22
B14	25	4125	0.067	0.008	10.0	7.61	↑	−15.04
B15	25	4125	0.064	0.008	8.7	7.61	↑	−15.15
B16	25	4125	0.056	0.008	10.5	7.55	↑	−15.20
C12	50	4125	0.209	0.016	10.7	7.66	↑	−13.70

APPENDIX TABLE 1. *Continued*

Sample	T (°C)	Time (hours)	ΣSi (mm)	ΣAl (mm)	ΣNa (mm)	pH_{25}	Direction	$\log Q_i$
				Castle Creek Na-clinoptilolite				
1	125	339	4.20	0.11	3.04	6.84	↑	−19.02
2	125	339	3.74	0.06	2.59	6.84	↑	−19.60
3	125	339	4.44	0.11	2.44	6.84	↑	−19.02
4	175	170	7.24	0.41	3.65	8.31	↑	−16.97
5	225	103	12.51	0.54	4.02	8.63	↑	−15.65
7	265	77	18.67	0.51	4.27	8.80	↑	−14.83
8	265	77	16.24	0.58	4.20	8.80	↑	−15.07
9	200	96	11.43	2.02	0.29	8.76	↓	−16.45
10	200	96	9.49	0.32	1.93	8.76	↓	−16.82
11	175	122	8.46	0.38	1.33	8.74	↓	−17.15
12	175	122	10.19	0.21	1.43	8.74	↓	−16.99
13	125	280	7.62	0.07	1.14	8.81	↓	−18.25
14	125	280	6.69	0.18	1.11	8.81	↓	−18.08
16	225	245	15.72	0.36	1.61	8.44	↑	−15.80
17	225	245	16.20	0.74	1.85	8.44	↑	−15.33
23	90	1080	3.62	0.02	0.23	7.36	↑	−21.23
24	90	1080	3.60	0.02	0.33	7.36	↑	−21.11
55	100	360	3.34	0.09	0.65	8.21	↑	−20.09
56	100	360	3.45	0.05	0.59	8.21	↑	−20.34
74	100	697	3.98	0.19	0.84	8.91	↑	−19.25
75	100	697	3.49	0.19	0.72	8.91	↑	−19.61
79	125	122	5.21	0.30	1.18	8.24	↑	−18.30
80	125	338	5.20	0.35	1.26	8.49	↑	−18.19
81	125	338	5.08	0.31	1.22	8.49	↑	−18.31
85	125	407	5.00	0.33	1.22	8.51	↑	−18.32
87	125	465	4.81	0.29	1.23	8.53	↑	−18.46
89	125	625	4.91	0.29	1.44	8.51	↑	−18.35
91	100	48	4.36	0.17	1.17	8.47	↓	−18.96
92	100	216	4.04	0.13	1.11	8.49	↓	−19.26
95	100	885	3.61	0.15	1.09	8.53	↓	−19.46
B6	25	3288	0.10	0.004	9.35	8.42	↑	−27.81
B7	25	3288	0.13	0.004	9.27	8.42	↑	−27.28
C6	50	2520	0.34	0.008	10.90	7.63	↑	−24.79
C7	50	2520	0.36	0.008	11.38	7.63	↑	−24.65
B17	25	4125	0.11	0.012	8.91	7.48	↑	−27.08
B18	25	4125	0.12	0.008	9.45	7.55	↑	−27.05
C13	50	4125	0.32	0.027	9.73	7.59	↑	−24.39
C14	50	4125	0.30	0.031	9.82	7.59	↑	−24.45
D1	25	5125	0.15	0.016	10.23	7.25	↑	−26.39
D2	25	5126	0.14	0.020	10.15	7.25	↑	−26.23
D3	50	5126	0.33	0.027	10.09	7.36	↑	−24.34
D4	50	5126	0.34	0.031	9.95	7.36	↑	−24.34

Note: Direction of approach to equilibrium indicated by ↑ (undersaturation) or ↓ (supersaturation).

APPENDIX TABLE 2. Experimental solubility data for K-clinoptilolite

Sample	T (°C)	Time (hours)	ΣSi (mm)	ΣAl (mm)	ΣK (mm)	pH$_{25}$	Direction	log Q_i
				Castle Creek K-clinoptilolite				
93	125	357	3.25	0.07	0.46	8.21	↑	−20.48
94	125	357	3.15	0.03	0.44	8.21	↑	−20.89
96	175	75	6.67	0.13	0.58	7.96	↑	−18.55
97	175	75	6.50	0.10	0.53	7.96	↑	−18.77
98	200	52	9.21	0.14	0.74	8.49	↑	−17.73
99	225	44	11.71	0.20	0.83	8.29	↑	−16.98
100	225	44	11.53	0.18	0.82	8.29	↑	−17.07
101	265	20	15.87	0.34	1.09	8.05	↑	−15.97
102	225	33	12.31	0.16	0.81	8.16	↓	−16.99
103	200	46	10.47	0.12	0.71	8.23	↓	−17.51
104	175	67	8.28	0.04	0.63	8.14	↓	−18.62
105	125	78	6.49	0.02	0.54	8.40	↓	−19.61
106	90	260	5.29	0.002	0.54	8.21	↓	−21.09
107	90	260	5.20	0.001	0.52	8.21	↓	−21.57
B8	25	3288	0.21	0.004	0.05	7.75	↑	−28.70
B9	25	3288	0.20	0.004	0.06	7.75	↑	−28.72
C8	50	2520	0.42	0.007	0.09	7.61	↑	−26.65
C9	50	2520	0.47	0.007	0.10	7.61	↑	−26.41
B21	25	3350	0.05	0.015	4.97	6.52	↑	−28.99
B22	25	3350	0.04	0.019	4.81	6.50	↑	−29.26
B19	25	4125	0.03	0.016	5.10	6.62	↑	−29.77
B20	25	4125	0.03	0.023	5.32	6.55	↑	−29.55
C15	50	3350	0.13	0.027	4.97	7.01	↑	−26.62
C16	50	3350	0.14	0.035	4.99	7.01	↑	−26.38
C17	50	4125	0.14	0.035	4.89	6.89	↑	−26.39
C18	50	4125	0.21	0.031	5.08	6.89	↑	−25.50
D5	25	5126	0.07	0.020	5.02	7.15	↑	−28.04
D6	25	5126	0.08	0.021	5.10	7.15	↑	−27.80
D7	50	5126	0.23	0.046	5.08	7.03	↑	−25.15
D8	50	5126	0.22	0.043	5.24	7.03	↑	−26.26

Note: Direction of approach to equilibrium indicated by ↑ (undersaturation) or ↓ (supersaturation).